Chinese Journal of Natural Medicines

Dietary titanium dioxide particles (E171) promote colitis-associated colorectal cancer development in mice through macrophage-derived S100A8/S100A9secretion mediated by NLRP3/Caspase 1/GSDMD pathway

Ping Wang, Yan Zhong, Jingquan Liu, Lingfang Gao, Ting Long, Zuguo Li

Citation: Ping Wang, Yan Zhong, Jingquan Liu, Lingfang Gao, Ting Long, Zuguo Li, Dietary titanium dioxide particles (E171) promote colitis-associated colorectal cancer development in mice through macrophage-derived S100A8/S100A9secretion mediated by NLRP3/Caspase 1/GSDMD pathway, Chinese Journal of Natural Medicines, 2026, 24(2), 215-226. doi: 10.1016/S1875-5364(26)61092-8.

View online: https://doi.org/10.1016/S1875-5364(26)61092-8

Chinese Journal of Natural Medicines 24 (2026) 215-226

Contents lists available at ScienceDirect

Chinese Journal of Natural Medicines

journal homepage: www.cjnmcpu.com/

Original article

Dietary titanium dioxide particles (E171) promote colitis-associated colorectal cancer development in mice through macrophage-derived S100A8/S100A9 secretion mediated by NLRP3/Caspase 1/GSDMD pathway

Ping Wang[a,b,c], Yan Zhong[a,b], Jingquan Liu[a,b], Lingfang Gao[a], Ting Long[a], Zuguo Li[a,b,*]

[a] *Department of Pathology, Shenzhen Hospital, Southern Medical University, Shenzhen 518101, China*
[b] *Department of Pathology, School of Basic Medical Sciences, Southern Medical University, Guangzhou 510515, China*
[c] *Department of Pathology, The First Affiliated Hospital of Guangzhou Medical University, National Clinical Centre for Respiratory Disease, Guangzhou 510120, China.*

ARTICLE INFO

Article history:
Received 7 January 2025
Revised 21 March 2025
Accepted 24 June 2025
Available online 20 February 2026

Keywords:
Titanium dioxide particles (E171)
Colitis-associated colorectal cancer
Macrophage
S100A8/S100A9
NLRP3/Caspase 1/GSDMD

ABSTRACT

Colitis-associated colorectal cancer (CAC) is a major contributor to cancer-related mortality worldwide. Titanium dioxide (TiO_2, E171), a widely used food additive, has been insufficiently studied regarding its effects on macrophages within colon tumors during CAC development. In this study, CAC mouse models were used to investigate the biological impact of dietary E171 on macrophages *in vivo*, while lipopolysaccharide (LPS)-stimulated RAW264.7 macrophage cell lines were employed to elucidate the underlying mechanisms *in vitro*. We found that dietary E171 intake accelerated CAC development, exacerbated inflammatory responses and oxidative stress, and upregulated CAC-associated genes, including *S100a8*, *S100a9*, *Lcn2*, *S100a11*, *Cxcl2*, and *interleukin-1α* (*Il-1α*). E171 also increased the expression of S100A8, S100A9, NOD-like receptor family pyrin domain-containing 3 (NLRP3), and gasdermin-D *N*-terminal (GSDMD-N) in macrophages within colon tumors. In inflammatory macrophages, E171 exposure enhanced cell viability, increased reactive oxygen species (ROS) levels, and elevated the expression and secretion of S100A8 and S100A9, consistent with *in vivo* histological observations. Furthermore, E171-induced secretion of S100A8 and S100A9 in macrophages was suppressed by specific inhibitors, including *N*-acetylcysteine (NAC, ROS inhibitor), MCC950 (NLRP3 inhibitor), Z-YVAD-FMK (caspase 1 inhibitor), disulfiram (GSDMD inhibitor), and transfection of NLRP3 small interfering ribonucleic acid (siRNA). These results indicate that dietary E171 promotes CAC development by activating macrophages, with S100A8 and S100A9 serving as key mediators, and the NLRP3/caspase 1/GSDMD pathway acting as a critical mechanism.

1. Introduction

Colorectal cancer (CRC) is the third most prevalent cancer and the second leading cause of cancer-related deaths globally [1]. Evidence indicates that diet and chronic colon inflammation are key factors in the development of colitis-associated colorectal cancer (CAC) [2]. In particular, consumption of processed foods containing additives has been associated with carcinogenesis in the colon and rectum [3]. One such additive, food-grade titanium dioxide (TiO_2, E171), is widely used for its coloring and opacifying properties in over 900 processed food products, including chewing gum, sauces, pastries, ice creams, and candies [4, 5]. Given that TiO_2 has been classified as a possible carcinogen when inhaled, and considering growing concerns about the interaction between TiO_2 particles and the gastrointestinal tract, it is essential to evaluate the potential risks of dietary E171 in intestinal tumor development.

The mean particle size of E171 ranges from 106 to 132 nm, with over 36% of the particles measuring less than 100 nm in diameter [6]. E171 has been identified as a potential immunotoxin capable of inducing intestinal inflammation [7]. Previous studies have shown that intragastric administration of E171 exacerbates intestinal tumor development, possibly due to reduced goblet cell numbers [8]. However, in a model of dimethylhydrazine-induced carcinogenesis, E171 administered within a food matrix did not alter immune parameters or the tissue structure of the large intestine in rats [9]. Therefore, further in-depth research is required to clarify the immunotoxic mechanisms of dietary E171 in CAC.

Following ingestion, E171 particles reach the colon, where they may directly influence tumorigenesis [10]. In chronic inflammation, pro-inflammatory macrophages respond to environmental stimuli within the tumor microenvironment by producing chemokines, cytokines, and reactive oxygen species (ROS) [11, 12]. Prior studies have demonstrated that elevated ROS levels induced by TiO_2 nanoparticles (NPs) can activate nuclear factor kappa B (NF-κB), resulting in increased expression of pro-inflammatory genes in macrophages [13, 14]. Chronic colonic inflammation is also associated with damage-associated molecular patterns (DAMPs), such as S100A8 and S100A9, which contribute to CAC progression [15]. The NOD-like receptor family pyrin domain-containing 3 (NLRP3) inflammasome and gasdermin-D (GSDMD)

* Corresponding author.
E-mail address: lizg@smu.edu.cn (Z. Li)

https://doi.org/10.1016/S1875-5364(26)61092-8

pore formation play pivotal roles in inflammation and CAC development, exerting either protective or detrimental effects depending on cytokine-dependent pathways [16, 17]. However, the influence of E171 on the NLRP3-GSDMD signaling axis and its downstream cytokines in CAC-associated macrophages remains incompletely understood.

This study investigated the effects of E171 on macrophages within an inflammatory microenvironment using the azoxymethane (AOM)/dextran sodium sulfate (DSS)-induced C57BL/6J mouse model of CAC and lipopolysaccharide (LPS)-stimulated RAW264.7 mouse macrophages. The objective was to determine how E171 influences CAC development by examining its impact on macrophages in colitis-associated tumors. This work provides critical insights into the molecular factors and mechanisms underlying dietary E171-induced CAC progression.

2. Materials and methods

2.1. Preparation and characteristics

E171 particles were kindly provided by Sensient Technologies Company in China. The primary size and morphology of E171 particles were analyzed using transmission electron microscopy (TEM, JEM-2100F, JEOL, Japan). Crystal structures were determined by X-ray powder diffractometry (XRD, Rigaku Miniflex-II, Japan). Specific surface areas were measured using the Brunauer–Emmett–Teller (BET) method (Micromeritics ASAP 2020, USA). Hydrodynamic diameters and zeta potentials of E171 suspensions were measured using a Malvern Zetasizer (Nano-ZS, Malvern, UK).

For cell experiments, a stock solution of E171 was prepared by dispersing particles in phosphate-buffered saline (PBS) at a concentration of 1 mg·mL^{-1}, followed by autoclaving. Working solutions were prepared by diluting the stock in culture medium and were sonicated in an ice bath for 15 min prior to each use to ensure uniform dispersion.

2.2. Subjects and treatments

Seven-week-old male C57BL/6J mice were obtained from the Animal Center of Southern Medical University and housed under specific pathogen-free conditions at 23 ± 1.1 °C and 60% ± 10% humidity. The study was approved by the Bioethics Committee of Shenzhen Hospital of Southern Medical University (No. 2022-0132). Mice underwent a one-week acclimatization period before treatment. Animals were divided into four groups (n = 6): (1) control, (2) E171, (3) CAC, and (4) CAC + E171. CAC was induced by a single intraperitoneal injection of AOM (MP Biomedicals, US) at 10 mg·kg^{-1}. One week after AOM administration, mice received 2% DSS (MP Biomedicals, US) in drinking water for 7 days, followed by two weeks of regular water. This DSS cycle was repeated twice to establish CAC models [18]. Diets were formulated by Jiangsu Xietong Pharmaceutical Bio-engineering Co., Ltd. (Jiangsu, China), with E171 uniformly mixed into the feed using a commercial mixer. The dosage was based on previous studies [10, 19]. Fig. 1 outlines the experimental protocol. Disease activity index (DAI) was assessed weekly [20]. After 10 weeks, mice were euthanized. During necropsy, colon tissues were excised, longitudinally opened, photographed, and the tumor number and size were quantified using ImageJ software.

2.3. Culture and treatment of cells

The RAW264.7 macrophage cell line was obtained from Procell Life Science & Technology Co., Ltd. (Wuhan, China) and authenticated *via* STR profiling, confirming alignment with DSMZ reference data. Cells were cultured at 37 °C in a humidified incubator with 5% CO_2, using Dulbecco's modified Eagle medium supplemented with 10% fetal bovine serum and 1% penicillin-streptomycin. Cells were passaged at approximately 90% confluence, and culture medium was replaced every other day. Macrophages were stimulated with LPS (Sigma-Aldrich, US) at 100 ng·mL^{-1} [21]. LPS-stimulated RAW264.7 cells were co-treated with E171 working solutions at concentrations of 0, 12.5, 25, 50, 100, or 200 μg·mL^{-1} for durations of 1.5, 3, 6, 12, or 24 h.

2.4. TEM observation

Tissue samples (1 × 2 mm^2) were collected from freshly excised colorectal tumor regions using a sharp surgical blade. Specimens were fixed in 2.5% glutaraldehyde and incubated at 4 °C for 12 h. RAW264.7 cells were rinsed with PBS at 37 °C and fixed with 2.5% glutaraldehyde. After harvesting adherent macrophages by centrifugation at 1000 × g for 5 min at 4 °C, samples were embedded, and ultrathin sections were prepared. Ultrastructural features of colon tissues and cells were examined using TEM.

2.5. Histopathological examination

Colon tissues were fixed in 4% paraformaldehyde (Macklin, China) for 24 h, dehydrated through graded ethanol and xylene, and embedded in paraffin. Sections of 4 μm thickness were cut and subjected to hematoxylin and eosin (H&E) staining (Macklin, China). Colon inflammation was scored based on criteria for inflammatory cell infiltration [22], with average scores derived from ten fields at 400 × magnification. Immunohistochemical analysis was performed to detect protein expression using antibodies against S100A8, S100A9, cluster of differentiation 68 (CD68), CD80, CD163, and CD206 (all Proteintech, USA) and CD86 (ABclonal, USA). Images were captured using a Leica DM4B biological microscope. Staining intensity and area were quantified using ImageJ software.

2.6. Ribonucleic acid sequencing (RNA-seq)

Total RNA was extracted from colon tissues by Shanghai Majorbio Bio-pharm Biotechnology Co., Ltd. (Shanghai, China), followed by RNA purification, reverse transcription, library construction, and sequencing. Quality control and read mapping were performed according to Illumina (San Diego, CA) protocols. RNA-seq data and expression files were deposited in the NCBI GEO Database under accession PRJNA1041953. Differentially expressed genes (DEGs) were identified using DESeq, and transcript expression levels were calculated using the TPM method. Genes with $|\log_2$ fold change$| > 0$ and $P < 0.05$ were considered significantly differentially expressed.

2.7. Quantitative real-time polymerase chain reaction (qRT-PCR) analysis

TRIzol reagent (Thermo Fisher Scientific, USA) was used to extract RNA from colon tissues previously frozen in liquid nitrogen and stored at −80 °C. RNA purity and concentration were determined spectrophotometrically by absorbance at 260 and 280 nm (Thermo Fisher Scientific, USA). cDNA was synthesized using the PrimeScript^{TM} RT reagent kit (TaKaRa, Japan). qRT-PCR was performed using SYBR Premix Ex Taq (TaKaRa, Japan) on a 7500 Fast Real-Time PCR System (Applied Biosystems, Singapore). Gene expression levels were normalized to glyceraldehyde 3-phosphate dehydrogenase (GAPDH) using the $2^{-\Delta\Delta Ct}$ method. RAW264.7 cells were lysed following the same procedure as for colon tissues. Primer sequences for mouse genes used in qRT-

PCR are listed in Table 1.

2.8. Enzyme-linked immunosorbent assay (ELISA)

To quantify cytokine levels, mouse colon tissue homogenates were subjected to sonication and centrifuged at 5000 × *g* for 10 min to collect the supernatant. Macrophage culture supernatants were collected and centrifuged at 1000 × *g* for 10 min at 4 °C. The concentrations of S100A8, S100A9 (ELK Biotechnology, China), interleukin-1β (IL-1β), and IL-18 (Absin, China) were determined using ELISA kits according to the manufacturers' instructions. Results were expressed in $ng \cdot mL^{-1}$ or $pg \cdot mL^{-1}$, with concentrations calculated from standard curves generated from optical density (OD) readings. A microplate reader (Biotek SynergyH1, China) was used to measure absorbance for S100A8, S100A9, IL-1β, and IL-18.

2.9. Measurements of oxidative stress biomarkers

Frozen colon tissues stored in liquid nitrogen at −80 °C were homogenized in precooled normal saline using a tissue homogenizer. Protein concentrations in the supernatants (1∶10, *W*/*V*) were measured using a BCA protein assay kit (Elabscience, China). According to the manufacturer's protocols, the activities of catalase (CAT), glutathione peroxidase (GSH-Px), total superoxide dismutase (T-SOD), and malondialdehyde (MDA) levels were assessed using a microplate reader (Biotek SynergyH1, China) following the provided reagent procedures (Nanjing Jiancheng Bioengineering Institute, Nanjing, China).

2.10. Cell survival assay

RAW264.7 cells were seeded into 96-well plates at a density of 4×10^3 cells per well and incubated overnight to allow attachment. Cells were then treated with LPS and E171 particles. Cell viability was assessed using the cell counting kit-8 (CCK-8) assay kit (Dojindo, Japan), and absorbance was measured with a microplate reader (Biotek SynergyH1, China).

2.11. Cellular ROS assay

Intracellular ROS levels were measured using 2',7'-dichlorofluorescin diacetate (DCFH-DA) probes (Elabscience, China). After washing with PBS and detachment using EDTA-free trypsin, RAW264.7 cells were incubated with DCFH-DA (10 $mol \cdot L^{-1}$) for 30 min at 37 °C. Cells were then washed twice and resuspended in PBS. Fluorescence intensity was quantified using a microplate reader (Biotek SynergyH1, China) to reflect intracellular ROS levels.

2.12. Small interfering RNA (siRNA) transfection

SiRNAs targeting mouse NLRP3 were obtained from GenePharma (Suzhou, China). RAW264.7 cells were transiently transfected with siRNA using Lipofectamine 3000 Transfection Reagent (Invitrogen, US) according to the manufacturer's protocol. Table 2 lists the RNA interference oligonucleotide sequences used for siRNA transfection in mouse cells.

2.13. Inhibitor application

RAW264.7 cells were pretreated with inhibitors of ROS, NLRP3, caspase 1, and GSDMD for 3 h prior to E171 exposure for 12 h. *N*-acetylcysteine (NAC, 5 $\mu mol \cdot L^{-1}$; Selleck, US) was used as a ROS inhibitor. MCC950 (1 $\mu mol \cdot L^{-1}$; Selleck, US) served as an NLRP3 inhibitor. Z-YVAD-FMK (2 $\mu mol \cdot L^{-1}$; Selleck, US) was applied to inhibit caspase 1, and disulfiram (10 $\mu mol \cdot L^{-1}$; Selleck, US) was used to block GSDMD.

2.14. Immunofluorescence examination

For immunofluorescence staining, the following primary antibodies were used in the *in vivo* study: K18, S100A8, S100A9, CD68, F4/80, NLRP3 (all Proteintech, USA), Ki67, CD11b, myeloperoxidase (MPO), gasdermin-D *N*-terminal (GSDMD-N) (all Immunoway, USA), and 8-hydroxydeoxyguanosine (8-OHdG; Bioss, China). Cells were fixed with 4% paraformaldehyde overnight and permeabilized with 0.5% Triton X-100 for 15 min. After blocking with 5% bovine serum albumin (BSA) and 10% goat serum for 2 h, cells were incubated with primary antibodies against S100A8, S100A9, NLRP3 (all Proteintech, USA), phospho-NF-κB (p-NF-κB) p65, cleaved-caspase 1, and GSDMD-N (all Immunoway, USA) at 4 °C overnight. Subsequently, Alexa 488/594-conjugated secondary antibodies (FDbio, China) were applied. Fluorescence images were acquired using a DM4B fluorescence microscope (Leica, Germany). Positive cells were quantified using ImageJ software.

2.15. Western blot analysis

Total proteins were extracted from cells using RIPA lysis buffer supplemented with PMSF, protease inhibitors, and protein phosphatase inhibitors (all from FDbio, China). Protein concentrations were determined using BCA protein assay kits (Elab-

Table 1 Primer sequences specific to mice were used in the qRT-PCR analysis.

Gene	Forward primer	Reverse primer
S100a8	CCATGCCCTCTACAAGAATGACT	GCCACACCCACTTTTATCACC
S100a9	GCAGCATAACCACCATCATCATCGAC	CTGTGCTTCCACCATTTGTCTGA
S100a11	GCTGCCTTCACAAAGAACCAGA	GGAAATCTAGCTGCCCGTCAC
Lcn2	TCGCTACTGGATCAGAACATTTG	GAACTGGTTGTAGTCCGTGGTG
Cxcl2	CTGCCAAGGGTTGACTTCAAGA	CTTCAGGGTCAAGGCAAACT
Il-1α	TCAGCAACGTCAAGCAACGG	GGTGCTGATCTGGGTTGGATG
GAPDH	TGTGTCCGTCGTGGATCTGA	TTGCTGTTGAAGTCGCAGGAG

Table 2 List of RNA interference oligo sequences used for siRNA transfection.

siRNA	Sense 5′ to 3′	Anti-sense 5′ to 3′
NLRP3	CCAACUGGUCAAGGAGCAUTT	AUGCUCCUUGACCAGUUGGTT

science, China). Equal amounts of protein were separated by 10% SDS-PAGE and transferred onto PVDF membranes. Membranes were blocked with 5% BSA (FDbio, China) for 1 h and then incubated with primary antibodies targeting NF-κB p65, p-NF-κB p65, NLRP3, cleaved-caspase 1, GSDMD-N, IL-1β, IL-18 (all Immunoway, USA), S100A8, S100A9, and GAPDH (all Proteintech, USA) at 4 °C overnight. Following incubation with horseradish peroxidase-conjugated goat anti-rabbit or anti-mouse secondary antibodies (FDbio, China), protein bands were visualized using an ECL chemiluminescence solution (FDbio, China) and detected with a Tanon chemiluminescence imaging system (China). Band intensities were quantified using ImageJ software.

2.16. Statistical analysis

Data were analyzed using SPSS 18.0 and are presented as mean ± standard deviation (SD). Group comparisons were performed using one-way ANOVA followed by Bonferroni post hoc tests. A P-value < 0.05 was considered statistically significant. Graphs were generated using GraphPad Prism (version 9.0).

3. Results

3.1. Characterization and bio-transport of E171 particles

TEM imaging revealed that the E171 particles used in this study exhibited a typical spherical crystalline morphology (Fig. 1A). Their composition was confirmed by XRD (Fig. 1B). The average particle size was 107.9 ± 28.6 nm (Fig. 1C). Hydrodynamic diameters in DW and complete culture medium suspensions were 504.6 ± 16.7 and 493.4 ± 1.3 nm, respectively (Fig. 1D). Zeta potentials were measured at 6.9 ± 1.2 mV in DW and −25.6 ± 1.7 mV in complete medium (Fig. 1E). Specific surface area analysis yielded a value of 7.8 $m^2 \cdot g^{-1}$ for the E171 batch.

The experimental protocol for the mouse study is illustrated in Fig. 1F. To assess E171 localization within colonic tissues, TEM was performed on colon samples from control and CAC mice. While minimal E171 deposition was observed on the intestinal epithelium of normal mice (Fig. 1G), substantial accumulation was detected on the surface, within the cytoplasm, and in intercellular spaces of colon tumors in CAC mice (Figs. 1H–1J). This distinct distribution pattern suggests a potential role for dietary E171 in modulating the tumor microenvironment and promoting neoplastic progression. These comprehensive characterizations provide a solid foundation for investigating the biological effects of dietary E171 on colitis-associated colorectal carcinogenesis, ensuring that observed outcomes are attributable to well-defined physicochemical properties and biological interactions.

3.2. Dietary E171 aggravated pathological symptoms and promoted colon tumor development in CAC mice

Throughout the experiment, food and water intake remained consistent across all four groups (Supplementary Fig. S2), ruling out differential consumption as a confounding factor. Body weight changes were monitored to evaluate systemic effects. Control and E171-only mice exhibited steady weight gain, whereas CAC and CAC + E171 mice experienced weight loss during DSS administration, followed by recovery after DSS withdrawal. Notably, the CAC + E171 group maintained lower body weights compared to the CAC group even after DSS removal (Fig. 2A). Clinical disease activity was assessed *via* DAI scores. No symptoms were observed in control or E171-only mice. Both CAC and CAC + E171 groups showed elevated DAI scores during DSS treatment, which declined afterward; however, the CAC + E171 group exhibited significantly higher DAI scores than the CAC group, a difference that persisted post-DSS (Fig. 2B). Colon length, a surrogate marker of inflammation and tumorigenesis, was preserved in control and E171 groups but reduced in CAC mice, with further shortening in the CAC + E171 group (Figs. 2C and 2D). Tumor burden was absent in control and E171 mice, while both CAC groups developed tumors—larger and more numerous in the CAC + E171 group (Figs. 2E–2G).

Histopathological evaluation corroborated these findings. Control and E171 mice displayed intact colonic architecture without cytologic atypia. In contrast, CAC and CAC + E171 mice exhibited architectural distortion and cellular atypia, with more severe abnormalities in the E171-exposed group (Fig. 2H). Pathological mitoses, indicative of proliferative activity, were absent in control and E171 mice but present in both CAC groups, with a significantly higher mitosis index in the CAC + E171 group (Fig. 2I). Additionally, intestinal epithelial proliferation was assessed by $K18^+Ki67^+$ co-staining (Figs. 2J and 2K). The CAC + E171 group showed increased numbers of double-positive cells compared to the CAC group. Collectively, these results demonstrate that dietary E171 exacerbates colitis-associated tumorigenesis, evidenced by prolonged clinical symptoms, increased tumor burden, and enhanced cellular proliferation.

3.3. Dietary E171 exposure exacerbated inflammation and oxidative injury in CAC mice

TiO_2 NPs are known to promote inflammatory responses [23]. Control and E171-only mice showed no significant inflammatory infiltrates. In contrast, CAC mice exhibited immune cell infiltration in the lamina propria and submucosa of colon tumors, which was markedly intensified in the CAC + E171 group (Figs. 3A and 3B). To investigate the genomic impact of E171 on tumorigenesis, global transcriptome profiling was conducted in colon tissues from CAC and CAC + E171 mice (Fig. S2). A heatmap depicting hierarchical clustering of six pro-inflammatory and tumor-promoting DEGs is shown in Fig. 3C. E171 exposure led to significant upregulation of *S100a8*, *S100a9*, *Lcn2*, *S100a11*, *Cxcl2*, and *Il-1α* in colon tissues. qRT-PCR analysis confirmed elevated messenger RNA (mRNA) levels of all six genes in CAC mice compared to controls, with further increases in the CAC + E171 group (Fig. 3D).

In addition to inflammation, oxidative stress is a hallmark of TiO_2 NP toxicity [24]. Oxidative stress markers were evaluated in colon tumors (Fig. 3E). No differences were observed between control and E171-only mice. However, CAC mice exhibited decreased activities of CAT, GSH-Px, and T-SOD, along with increased MDA levels, indicating oxidative damage. These alterations were further exacerbated in the CAC + E171 group. 8-OHdG expression, a marker of oxidative DNA damage [25,26], was also assessed. The number of $8\text{-}OHdG^+$ cells in the lamina propria and submucosa was significantly higher in CAC mice than in controls and further increased in the CAC + E171 group (Figs. 3F and 3G). These findings confirm that oral E171 intake aggravates both inflammation and oxidative injury during colitis-associated tumorigenesis.

3.4. Dietary E171 exposure increased the expression of *S100A8*, *S100A9*, *NLRP3*, and *GSDMD-N* in the macrophages within colon tumors

Transcriptomic analysis identified *S100a8* and *S100a9* as the two most significantly upregulated genes among selected DEGs (Supplementary Fig. S2). ELISA quantification confirmed elevated S100A8 and S100A9 protein levels in colon tissues: higher in CAC mice than controls, and further increased in the CAC + E171 group (Fig. 4A). Immunohistochemistry revealed that $S100A8^+$ and $S100A9^+$ signals were predominantly localized in the lamina propria and submucosa of colon tumors (Fig. 4B). While only a few positive cells were detected in CAC mice, the CAC + E171 group exhibited a marked increase (Fig. 4C).

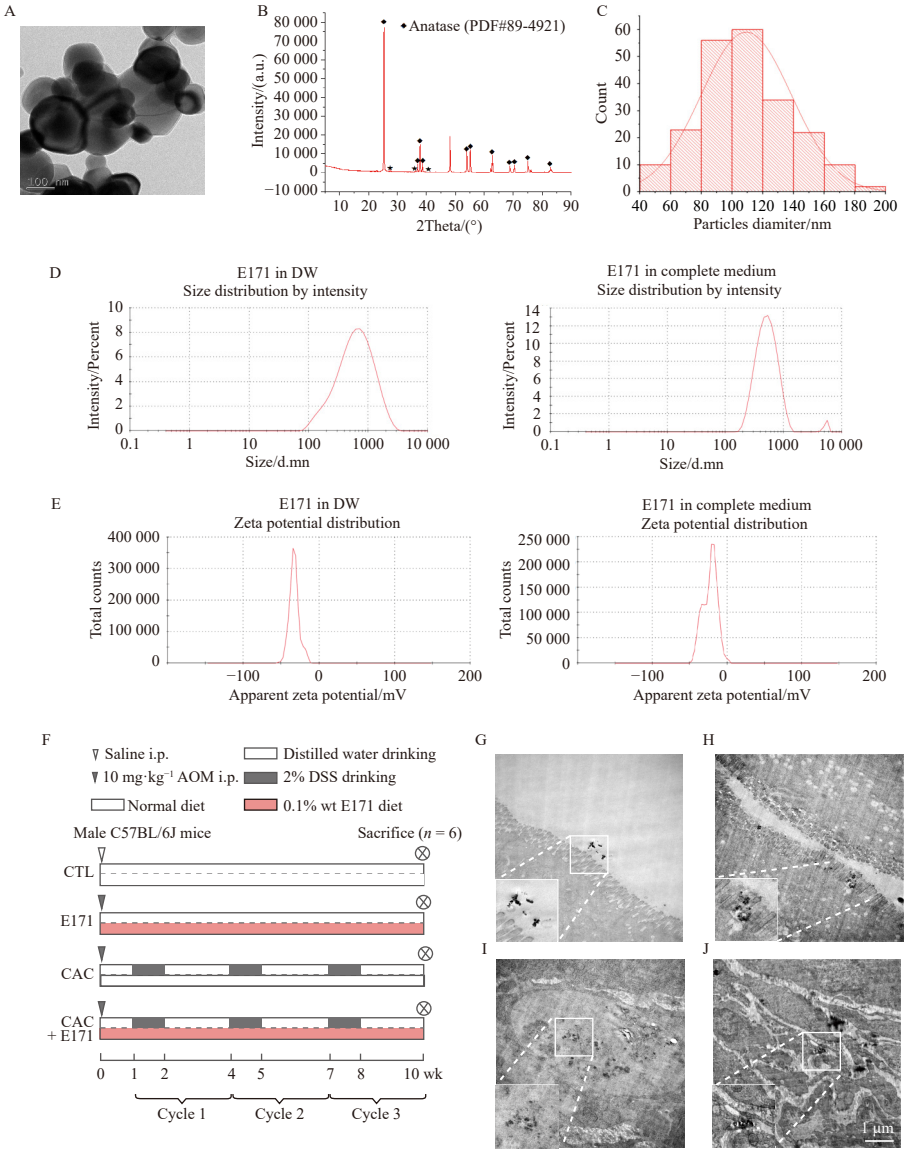

Fig. 1 Characterization of E171 and its penetration into colon tumor tissues. (A) TEM images of E171. (B) The X-ray diffraction spectrum confirming the composition of E171. (C) Particle size distribution of E171 (n = 314). (D) The hydrodynamic diameter of E171 in distilled water (DW) and complete medium. (E) The zeta potential measurements of E171 in DW and complete medium. (F) Schematic diagram of the *in vivo* experimental protocol. (G) TEM images of E171 in colitis-associated colon tumor tissues, observed on the epithelial surface (H), within the cytoplasm of epithelial cells (I), and in the intercellular space (J) (scale bar = 1 μm).

S100A8 and S100A9 are primarily produced by myeloid cells [27]. To identify their cellular origin, double immunofluorescence staining was performed using CD11b, MPO, and CD68. Most S100A8$^+$ and S100A9$^+$ cells co-localized with CD68 (Fig. 4D). Macrophage polarization was further characterized using markers: CD80 and CD86 (pro-inflammatory), and CD163 and CD206 (anti-inflammatory) [28]. Serial sections from CAC and CAC + E171 tumors showed that CD68$^+$ cells predominantly expressed CD80 and CD86, indicating a pro-inflammatory phenotype (Supplementary Fig. S3).

F4/80, a specific marker for mature murine macrophages [29], was used to further define the source of S100A8 and S100A9. Co-localization analysis revealed that S100A8$^+$ and S100A9$^+$ cells in CAC + E171 mice were also F4/80$^+$, with significantly higher numbers of F4/80$^+$S100A8$^+$ and F4/80$^+$S100A9$^+$ cells compared to the CAC mice (Figs. 4E and 4F). Activation of the NLRP3-GSDMD pathway amplifies inflammation in chronic diseases [30, 31]. Immunofluorescence demonstrated that F4/80$^+$ macrophages in colon tumors were also positive for NLRP3 and GSDMD-N, with increased numbers in the CAC + E171 group (Figs. 4G and 4H).

3.5. E171 increased oxidative stress injury and S100A8/S100A9 expression in LPS-stimulated RAW264.7 cells

To elucidate the mechanism underlying macrophage activation in CAC tumors upon E171 exposure, CCK-8 assays were conducted in LPS-stimulated RAW264.7 cells (Fig. 5A). E171 at concentrations of 12.5–100 μg·mL^{-1} did not affect cell viability. However, 200 μg·mL^{-1} E171 significantly increased viability at 1.5, 3, 6, 12, and 24 h. ROS generation is a key mechanism in TiO_2 NP-induced toxicity [15, 16]. ROS levels were unchanged at ≤ 50 μg·mL^{-1}, increased at 100 μg·mL^{-1} (12 h), and significantly elevated at 200 μg·mL^{-1} across all time points, peaking at 12 h (Fig. 5B). TEM images showed E171 internalization by macrophages, accompanied by mitochondrial swelling and cristae disruption (Fig. 5C). ROS elevation activates NF-κB, leading to pro-inflammatory gene expression [13, 14]. Western blot analysis revealed that 200 μg·mL^{-1} E171 increased p-NF-κB p65 phosphorylation at 12 h (Figs. 5D and 5E). Immunofluorescence confirmed enhanced nuclear translocation of p-NF-κB (Fig. 5F). qRT-PCR showed that 200 μg·mL^{-1} E171 upregulated *S100a8* and *S100a9* mRNA at 12 h (Fig. 5G). Immunofluorescence also demonstrated increased

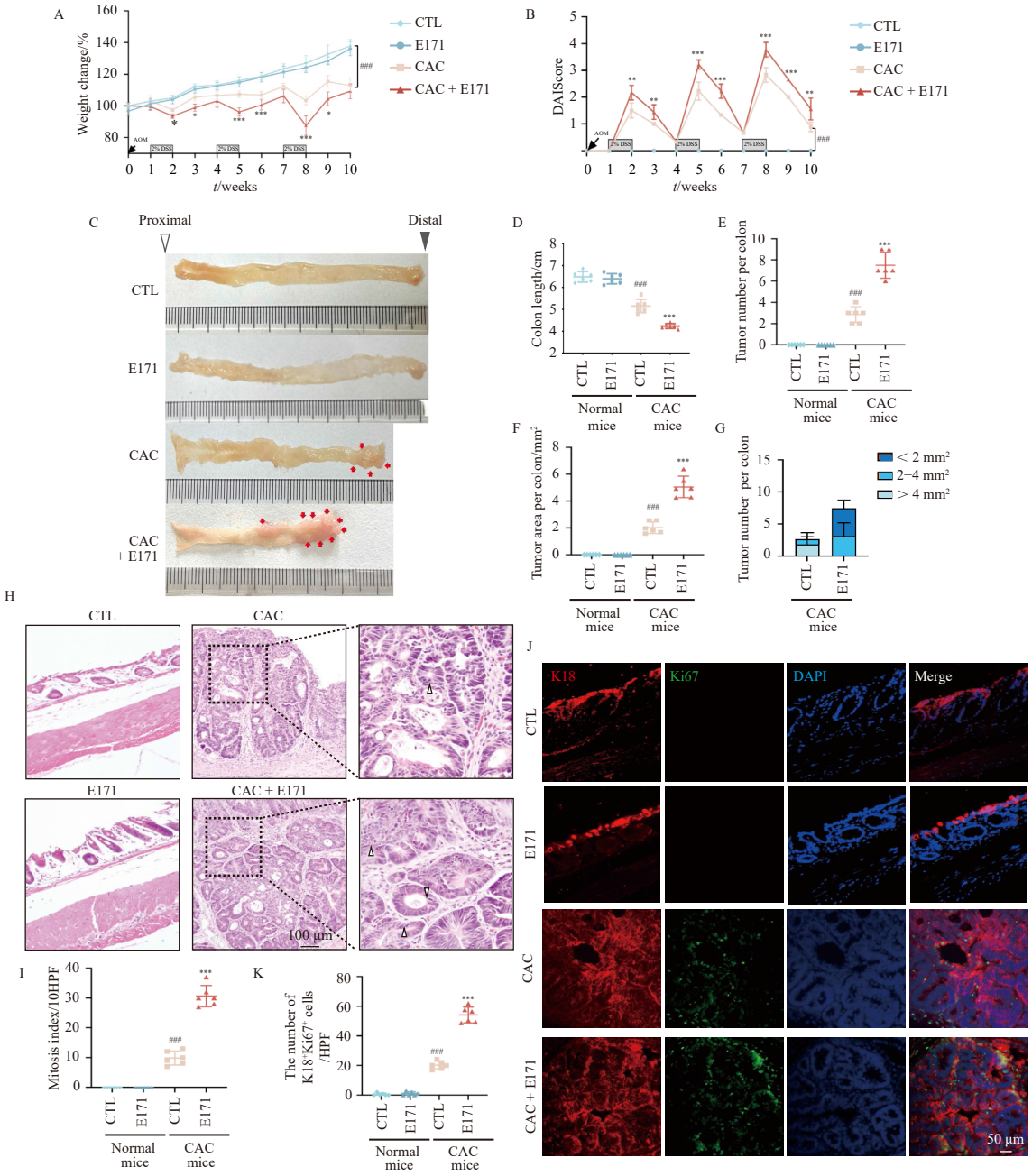

Fig. 2 Effects of dietary E171 on pathological symptoms and tumorigenesis in CAC mice. (A) Body weight changes. (B) DAI scores. (C) Gross morphology of colon tissues. Red arrows indicate visible tumor nodules. (D) Colon length. (E–G) Quantitative analysis of tumor number, size distribution (< 2 mm^2, 2–4 mm^2, > 4 mm^2), and incidence (H) H&E staining of colon tissue sections. White arrowheads indicate mitotic figures (scale bar = 100 μm). (I) Quantitative analysis of mitotic index based on H&E-stained sections. (J) Immunofluorescence staining of $K18^+Ki67^+$ cells in colon tissues. (K) Quantitative analysis of $K18^+Ki67^+$ cells in colon tissues (scale bar = 50 μm). Data are presented as mean ± SD (n = 6). $^{###}P < 0.001$ *vs* the control group; $^{*}P < 0.05$, $^{**}P < 0.01$ and $^{***}P < 0.001$ *vs* the CAC group.

S100A8 and S100A9 protein expression at 12 h (Figs. 5H and 5I).

3.6. E171-induced secretion of S100A8/S100A9 was mediated by the NLRP3/caspase 1/GSDMD pathway in LPS-stimulated RAW264.7 cells

S100A8 and S100A9 are secreted during inflammatory responses [30, 31]. ELISA showed that 200 $μg·mL^{-1}$ E171 increased S100A8 and S100A9 secretion after 12 h (Fig. 6A). Given the *in vivo* evidence of NLRP3-GSDMD pathway activation, we investigated its involvement *in vitro*. Western blot analysis revealed that E171 treatment significantly increased NLRP3, cleaved caspase 1, GSDMD-N, IL-1β, and IL-18 expression (Figs. 6B and 6C). Immunofluorescence confirmed elevated NLRP3, cleaved caspase 1, and GSDMD-N (Figs. 6D–6F). ELISA also showed increased IL-1β and IL-18 levels (Supplementary Fig. S4). To assess the role of ROS, cells were pretreated with NAC before E171 exposure. NAC significantly reduced NLRP3, cleaved caspase 1, and GSDMD-N expression (Figs. 6G and 6H). Furthermore, inhibition of ROS (NAC), NLRP3 (MCC950), caspase 1 (Z-YVAD-FMK), GSDMD (disulfiram), or NLRP3 knockdown *via* siRNA all suppressed E171-induced S100A8/S100A9 secretion (Fig. 6I). These results indicate that E171 promotes S100A8/S100A9 release in inflammatory macrophages *via* the ROS-dependent NLRP3/caspase 1/GSDMD pathway.

4. Discussion

The global incidence of CAC is increasing, though etiological factors remain incompletely understood. Diet plays a pivotal role

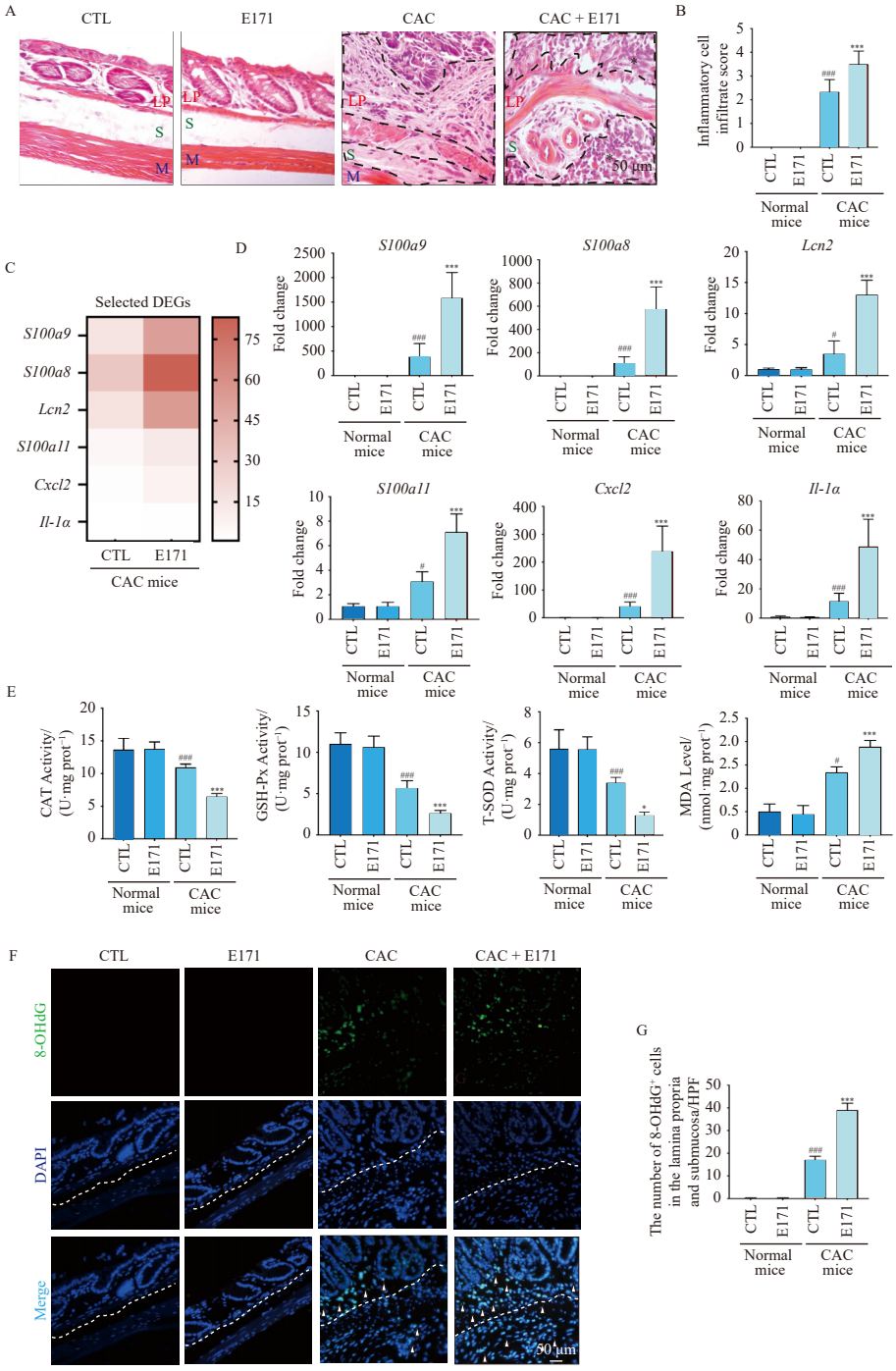

Fig. 3 Effects of dietary E171 on inflammation and oxidative stress in CAC mice. (A) Histological assessment of inflammatory cell infiltration in colon tissues *via* H&E staining. LP, lamina propria; S, submucosa; M, muscularis (scale bar = 50 μm). (B) Inflammatory cell infiltration scores. (C) A heatmap of differentially expressed genes (DEGs) related to inflammation and tumorigenesis (n = 3). (D) Relative mRNA expression levels of DEGs, measured by qRT-PCR and normalized to GAPDH expression levels. (E) The CAT, GSH-Px, T-SOD, and MDA levels in colon tissues. (F) Immunofluorescence staining of 8-OHdG in colon tissues. White dotted lines represent the boundary between the lamina propria and submucosa. White arrowheads indicate 8-OHdG$^+$ cells. (G) Quantitative analysis of 8-OHdG$^+$ cells in the lamina propria and submucosa of colon tissues (scale bar = 50 μm). Data are presented as mean ± SD (n = 6). $^{\#}P < 0.05$ and $^{\#\#\#}P < 0.001$ *vs* the control group; $^{*}P < 0.05$ and $^{***}P < 0.001$ *vs* the CAC group.

in CAC pathogenesis, and growing evidence suggests that E171, a widely used food additive, may contribute to disease risk. In this study, AOM/DSS-induced CAC mouse models were fed a diet containing E171, mimicking human dietary exposure [10, 19]. DSS-induced intestinal barrier disruption likely facilitated TiO_2 particle absorption [23], as confirmed by TEM detection of E171 retention in colon tumors. Although E171 alone did not induce tumors in healthy mice, it significantly increased tumor number and size in CAC mice. Histopathological analysis revealed enhanced tumor cell proliferation, evidenced by increased mitotic figures and K18$^+$Ki67$^+$ cells. These findings suggest that dietary E171 promotes CAC progression.

Despite extensive research on TiO_2 particles, few studies have explored the immunotoxic mechanisms of dietary E171 in CAC. Chronic inflammation drives CAC [12]. Here, E171 increased DAI scores during DSS treatment, indicating worsened colitis, and was associated with colon shortening and thickening. TiO_2 is known to enhance inflammatory cell recruitment. Histology confirmed intensified infiltration in the lamina propria and submucosa of E171-treated tumors. RNA-seq analysis revealed upregulation of pro-inflammatory mediators, including *S100a8*, *S100a9*, *Lcn2*, *S100a11*, *Cxcl2*, and *Il-1α*, all implicated in CAC pathogenesis [21, 32-36]. Both transcriptomic and qRT-PCR data confirmed E171-induced upregulation of these genes.

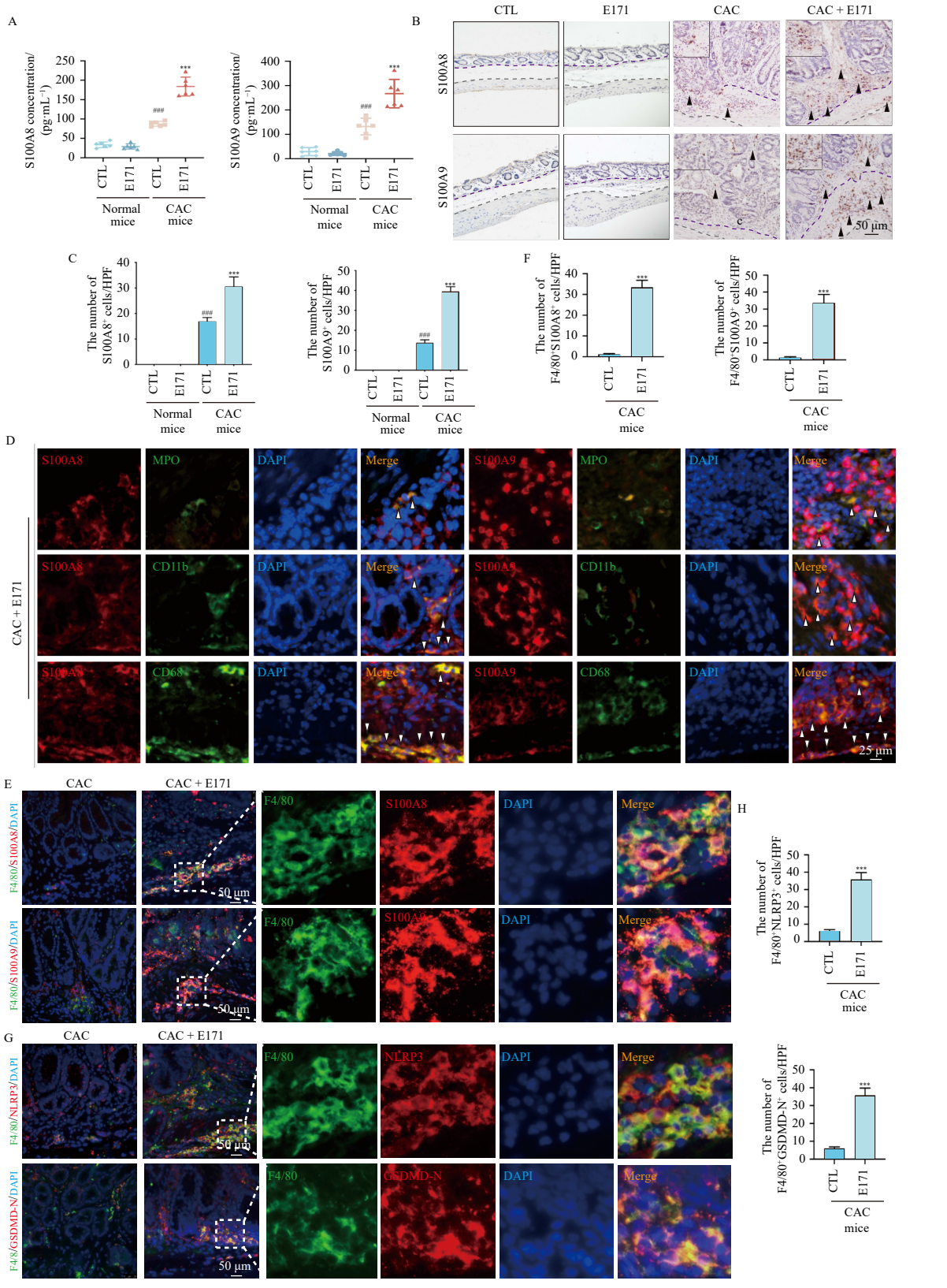

Fig. 4 Expressions of S100A8, S100A9, NLRP3, and GSDMD-N in colon tumors. (A) Protein levels of S100A8 and S100A9 in colon tissues measured by ELISA. (B) Immunohistochemistry images and (C) quantitative analysis of S100A8 and S100A9 expressions in the lamina propria and submucosa of colon tissues. The purple dotted lines represent the boundary of the lamina propria and submucosa. The gray dotted lines represent the boundary of the submucosa and muscularis. Black arrowheads indicate positive cells (scale bar = 100 μm). (D) Immunofluorescence staining of $CD11b^+S100A8^+$, $CD11b^+S100A9^+$, $MPO^+S100A8^+$, $MPO^+S100A9^+$, $CD68^+S100A8^+$, and $CD68^+S100A9^+$ in colon tumors. White arrowheads indicate double-positive cells (scale bar = 25 μm). (E) Immunofluorescence image and (F) quantitative analysis of $F4/80^+S100A8^+$ and $F4/80^+S100A9^+$ cells in colon tumors (scale bar = 50 μm). (G) Immunofluorescence images and (H) quantitative analysis of $F4/80^+NLRP3^+$ and $F4/80^+GSDMD\text{-}N^+$ cells in colon tumors. Data are presented as mean ± SD (n = 6). $^{###}P < 0.001$ *vs* the control group; $^{***}P < 0.001$ *vs* the CAC group.

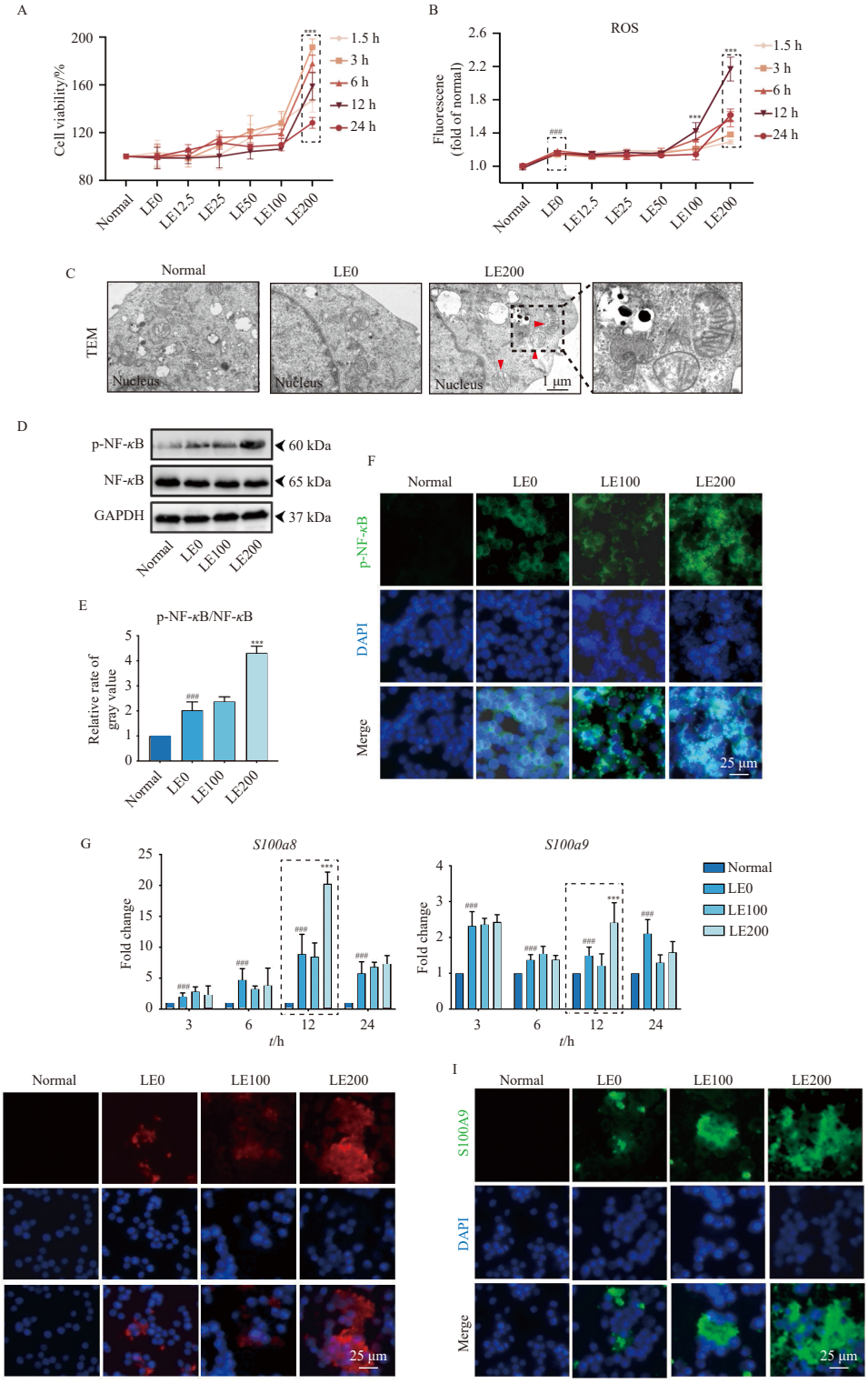

Fig. 5 Oxidative stress and S100A8 and S100A9 change induced by E171 in LPS-stimulated RAW264.7 cells. (A) The viability of RAW264.7 cells treated with LPS and various concentrations of E171, assessed by CCK-8 assay (n = 6). (B) Intracellular ROS levels of RAW264.7 measured using the DCFH-DA fluorescent probe. (C) TEM images of RAW264.7 cells exposed to LPS and 200 μg·mL^{-1} E171 for 12 h. E171 was engulfed by LPS-stimulated cells, resulting in mitochondrial structural alterations (red arrows) (scale bar = 1 μm). (D) The protein levels of NF-κB and p-NF-κB in RAW264.7 cells measured by Western blot. (E) Quantitation of the ratio of p-NF-κB/NF-κB in RAW264.7 cells. (F) Immunofluorescence determined the protein expression of p-NF-κB in RAW264.7 cells. (G) mRNA expression levels of *S100a8* and *S100a9* measured by qRT-PCR. (H and I) Immunofluorescence staining of S100A8 and S100A9 protein expression in RAW264.7 cells (scale bar = 25 μm). Data are presented as mean ± SD (n = 3). $^{###}P$ < 0.001 *vs* the normal group; $^{*}P$ < 0.05 and $^{***}P$ < 0.001 *vs* the LPS group (LE0). LE12.5, LE25, LE50, LE100, and LE200 indicate E171 treatment concentrations of 12.5, 25, 50, 100, and 200 μg·mL^{-1}, resepectively.

Recent studies highlight the interplay between chronic inflammation and oxidative stress in inflammation-driven cancers [37]. Our results show that E171 disrupts redox balance, reducing anti-oxidant enzyme activities (CAT, SOD, GSH-Px) and increasing MDA and 8-OHdG levels in colon tumors. Thus, E171 exacerbates oxidative damage in CAC.

S100A8 and S100A9, alarmins linked to inflammation and oxidative stress, are implicated in colorectal carcinogenesis [15, 21, 32, 33]. Transcriptomic and qRT-PCR analyses identified them as the most upregulated genes in E171-exposed CAC mice. We further

demonstrated that E171 enhances S100A8/S100A9 expression and secretion in colitis-associated tumors. These proteins are primarily expressed in myeloid cells [26, 38]. Co-localization studies showed that elevated S100A8/S100A9 in E171-exposed tumors originated from macrophages ($CD68^+/F4/80^+$), which exhibited a pro-inflammatory phenotype ($CD80^+/CD86^+$). Hence, E171 promotes macrophage-derived S100A8/S100A9 in CAC.

Macrophages respond robustly to environmental stimuli by generating ROS and amplifying inflammation [11], processes critical in CAC [12]. To further explore the mechanisms of E171 in promoting CAC, we used LPS-stimulated macrophages as an *in vitro* inflammation model. Particle characteristics can influence cellular uptake [39, 40]. Correa Segura et al. suggested that E171 particles induce mitochondrial permeability and cardiac damage after oral exposure in rats [41]. Colin-Val et al. found that mitophagy-related mitochondrial alterations were detected after E171 exposure [42]. Moreover, the cytotoxic and inflammatory potential of NPs is determined by the accumulation of ROS, a process that can be mediated through the activation of the NF-κB pathway [43]. *In vitro* study, when E171 concentration was below 100 $\mu g \cdot mL^{-1}$, cell viability and ROS levels remained unaffected; however, at 200 $\mu g \cdot mL^{-1}$, both cell viability and ROS levels significantly increased. The ROS levels peaked at 12 h after treatment with E171, accompanied by evident mitochondrial damage. Furthermore, treatment with 200 $\mu g \cdot mL^{-1}$ E171 at 12 h significantly promoted the nuclear translocation of p-NFκB and increased the transcription and expression of S100A8 and S100A9. Mitochondrial damage and the generation of ROS are also implicated in the activation of the NLRP3 inflammasome [44], which has been studied in RAW264.7 cells [45-47]. A positive feedback loop between S100A8/A9 and the NLRP3-GSDMD pathway reinforces innate immunity [31]. Thus, S100A8 and S100A9 can be activated as inflammatory factors and agonists of the NLRP3-GSDMD pathway involved in the inflammatory response. The activation of the NLRP3-GSDMD pathway in innate immune cells entails a two-step process: the initial signal induces NF-κB activation, while the subsequent signal prompts rapid caspase-1 activation *via* NLRP3, culminating in the cleavage of pro-IL-1β and pro-IL-18 [48]. The active caspase-1 subsequently cleaves GSDMD, producing an active *N*-terminal fragment that oligomerizes to form pores, and these pores facilitate the release of IL-1β and IL-18 [49]. *In vivo*, E171 increased $NLRP3^+$ and GSDMD-N^+ macrophages in tumors. *In vitro*, E171 activated this pathway in macrophages. S100A8/A9 secretion may share mechanistic similarities with IL-1β release [38]. Pretreatment with NAC or use of specific inhibitors and NLRP3 siRNA all attenuated S100A8/S100A9 secretion, confirming that E171 promotes their release *via* the ROS-NLRP3-caspase 1-GSDMD axis, thereby contributing to CAC progression.

5. Conclusions

In summary, dietary E171 exacerbates colitis-associated colon tumorigenesis in a mouse model by enhancing macrophage-derived S100A8 and S100A9 expression (Fig. 7). E171 promotes

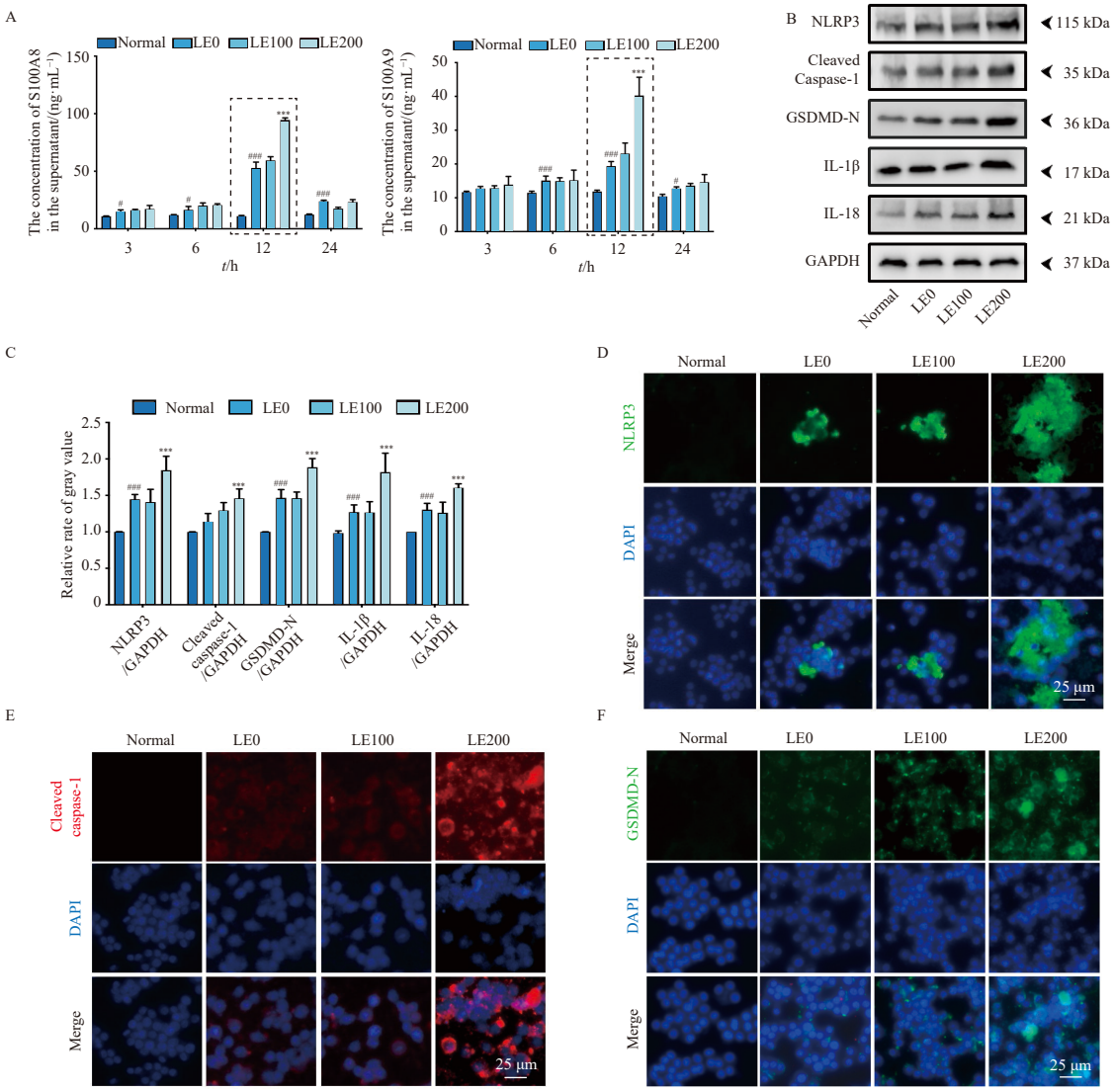

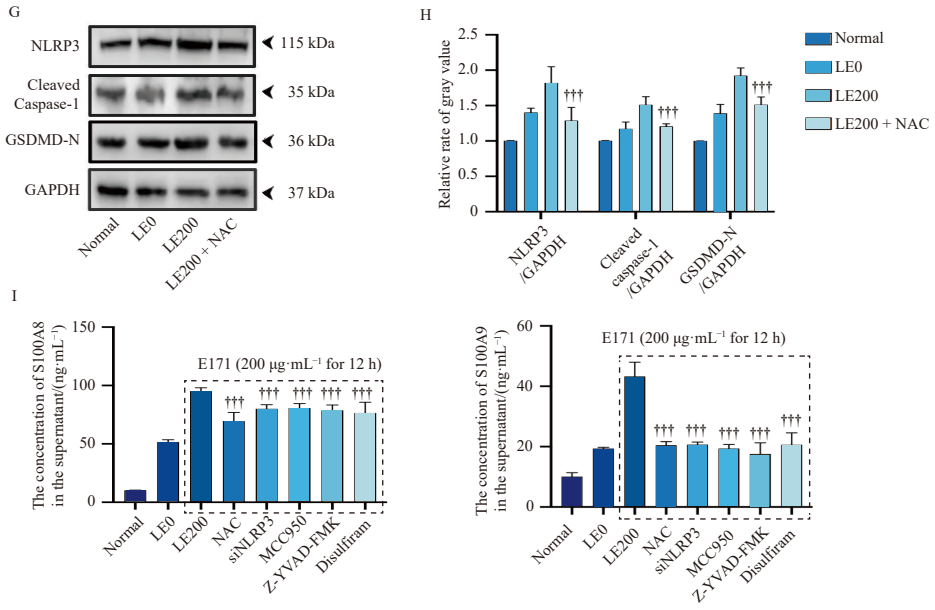

Fig. 6 E171-induced secretion of S100A8/A9 and activation of the NLRP3/caspase-1/GSDMD signaling pathway in LPS-stimulated RAW264.7 cells. (A) ELISA analysis of S100A8 and S100A9 protein levels in the supernatants of RAW264.7 cells treated with LPS and varying concentrations of E171. (B) Western blot detection of NLRP3, cleaved caspase-1, GSDMD-N, IL-1β, and IL-18 protein expression in cell lysates. (C) Quantitation of the protein levels of NLRP3, cleaved caspase-1, GSDMD-N, IL-1β, and IL-18. (D–F) Immunofluorescence staining of NLRP3, cleaved caspase-1, and GSDMD-N in RAW264.7 cells (scale bar = 25 μm). (G) Western blot analysis of NLRP3, cleaved caspase-1, and GSDMD-N in LPS and E171-treated RAW264.7 cells pre-treated with NAC treatment. (H) Quantitation of the protein levels of NLRP3, cleaved caspase-1, and GSDMD-N. (I) ELISA measurement of secreted S100A8 and S100A9 in the supernatants of cells treated with NAC, siNLRP3, MCC950, Z-YVAD-FMK, and disulfiram. Data are presented as mean ± SD (n = 3). $^{\#}P < 0.05$ and $^{\#\#\#}P < 0.001$ *vs* the normal group; $^{***}P < 0.001$ *vs* the LE0 group; $^{\dagger\dagger\dagger}P < 0.001$ *vs* the LE200 group.

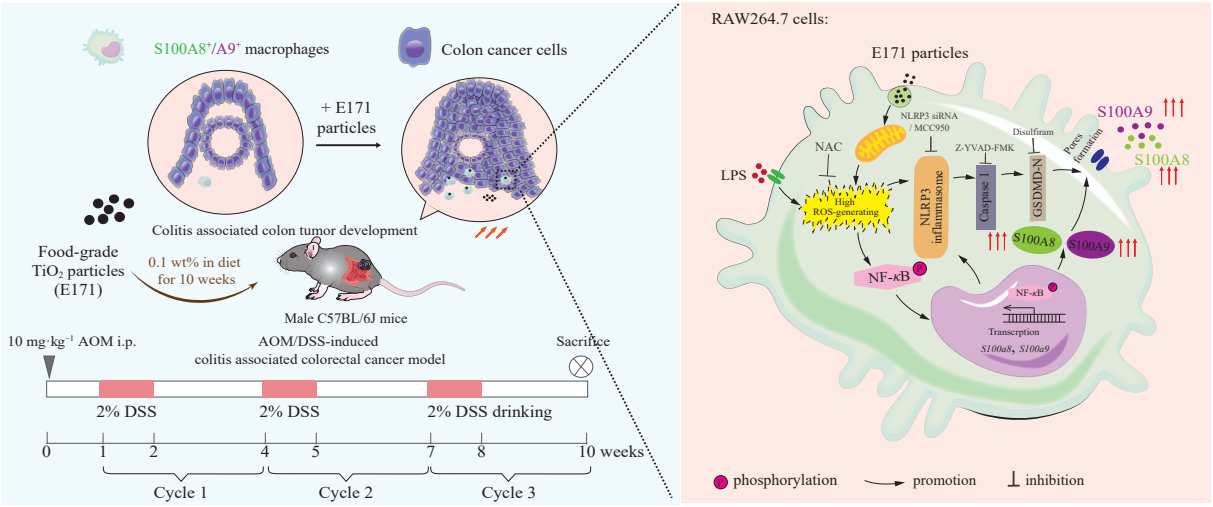

Fig. 7 A schematic illustration showing the impact of E171 particles on macrophages in CAC. In AOM/DSS-induced CAC mice, oral consumption (0.1 wt% in the diet for 10 weeks) of E171 particles promotes the colitis-associated colon tumor development and increases the infiltration of S100A8/A9-expressing macrophages. Moreover, E171 particles induce the secretion of S100A8 and S100A9 in LPS-stimulated RAW264.7 cells through the activation of the NLRP3/caspase-1/GSDMD pathway, which is mediated by elevated levels of ROS.

the secretion of these alarmins through oxidative stress-induced activation of the NLRP3/caspase 1/GSDMD pathway, both *in vivo* and *in vitro*. This study identifies key molecular mediators and mechanisms underlying E171's tumor-promoting effects in CAC, providing new insights into its pathogenicity.

Funding

This study was supported by the National Natural Science Foundation of China (Nos. 81974441 and 82203619) and the Science and Technology Planning Project of Shenzhen Municipality (Nos. JCYJ20190814105619048 and JCYJ20220530154202005).

Supporting information

Supporting information for this work can be obtained by contacting the corresponding authors *via* E-mail.

Declaration of conflicting interests

The authors declared no potential conflicts of interest with respect to the research, authorship, and/or publication of this article.

References

1 Siegel RL, Wagle NS, Cercek A, et al. Colorectal cancer statistics, 2023. *CA Cancer J Clin*. 2023;73(3):233-254. https://doi.org/10.3322/caac.21772.
2 Wesselink E, Boshuizen HC, van Lanen AS, et al. Dietary and lifestyle inflammation scores in relation to colorectal cancer recurrence and all-cause mortality: a longitudinal analysis. *Clin Nutr*. 2024;43(9):2092-2101. https://doi.org/10.1016/j.clnu.2024.07.028.
3 Vernia F, Longo S, Stefanelli G, et al. Dietary factors modulating colorectal carcinogenesis. *Nutrients*. 2021;13(1):143. https://doi.org/10.3390/

nu13010143.
4 Martirosyan A, Schneider YJ. Engineered nanomaterials in food: implications for food safety and consumer health. *Int J Environ Res Public Health*. 2014;11(6):5720-5750. https://doi.org/10.3390/ijerph110605720.
5 Jovanovic B. Critical review of public health regulations of titanium dioxide, a human food additive. *Integr Environ Assess Manag*. 2015;11(1):10-20. https://doi.org/10.1002/ieam.1571.
6 Weir A, Westerhoff P, Fabricius L, et al. Titanium dioxide nanoparticles in food and personal care products. *Environ Sci Technol*. 2012;46(4):2242-2250. https://doi.org/10.1021/es204168d.
7 EFSA Panel on Food Additives and Flavourings, Younes M, Aquilina G, et al. Safety assessment of titanium dioxide (E171) as a food additive. *EFSA J*. 2021;19(5):e06585. https://doi.org/10.2903/j.efsa.2021.6585.
8 Urrutia-Ortega IM, Garduno-Balderas LG, Delgado-Buenrostro NL, et al. Food-grade titanium dioxide exposure exacerbates tumor formation in colitis associated cancer model. *Food Chem Toxicol*. 2016;93:20-31. https://doi.org/10.1016/j.fct.2016.04.014.
9 Blevins LK, Crawford RB, Bach A, et al. Evaluation of immunologic and intestinal effects in rats administered an E171-containing diet, a food grade titanium dioxide (TiO_2). *Food Chem Toxicol*. 2019;133:110793. https://doi.org/10.1016/j.fct.2019.110793.
10 Cao X, Han Y, Gu M, et al. Foodborne titanium dioxide nanoparticles induce stronger adverse effects in obese mice than non-obese mice: gut microbiota dysbiosis, colonic inflammation, and proteome alterations. *Small*. 2020;16(36):e2001858. https://doi.org/10.1002/smll.202001858.
11 Waldner MJ, Neurath MF. Mechanisms of immune signaling in colitis-associated cancer. *Cell Mol Gastroenterol Hepatol*. 2015;1(1):6-16. https://doi.org/10.1016/j.jcmgh.2014.11.006.
12 Hartnett L, Egan LJ. Inflammation, DNA methylation and colitis-associated cancer. *Carcinogenesis*. 2012;33(4):723-731. https://doi.org/10.1093/carcin/bgs006.
13 Schanen BC, Karakoti AS, Seal S, et al. Exposure to titanium dioxide nanomaterials provokes inflammation of an *in vitro* human immune construct. *ACS Nano*. 2009;3(9):2523-2532. https://doi.org/10.1021/nn900403h.
14 Giovanni M, Yue J, Zhang L, et al. Pro-inflammatory responses of RAW264.7 macrophages when treated with ultralow concentrations of silver, titanium dioxide, and zinc oxide nanoparticles. *J Hazard Mater*. 2015;297:146-152. https://doi.org/10.1016/j.jhazmat.2015.04.081.
15 Cho E, Mun SJ, Kim HK, et al. Colon-targeted S100A8/A9-specific peptide systems ameliorate colitis and colitis-associated colorectal cancer in mouse models. *Acta Pharmacol Sin*. 2024;45(3):581-593. https://doi.org/10.1038/s41401-023-01188-2.
16 Sharma BR, Kanneganti TD. Inflammasome signaling in colorectal cancer. *Transl Res*. 2023;252:45-52. https://doi.org/10.1016/j.trsl.2022.09.002.
17 Yu YQ, Gamez-Belmonte R, Patankar JV, et al. The role of programmed necrosis in colorectal cancer. *Cancers (Basel)*. 2022;14(17):4295. https://doi.org/10.3390/cancers14174295.
18 Parang B, Barrett CW, Williams CS. AOM/DSS model of colitis-associated cancer. *Methods Mol Biol*. 2016;1422:297-307. https://doi.org/10.1007/978-1-4939-3603-8_26.
19 Mu W, Wang Y, Huang C, et al. Effect of long-term intake of dietary titanium dioxide nanoparticles on intestine inflammation in mice. *J Agric Food Chem*. 2019;67(33):9382-9389. https://doi.org/10.1021/acs.jafc.9b02391.
20 Xing L, Fu L, Cao S, et al. The anti-inflammatory effect of bovine bone-gelatin-derived peptides in LPS-induced RAW264.7 macrophages cells and dextran sulfate sodium-induced C57BL/6 mice. *Nutrients*. 2022;14(7):1479. https://doi.org/10.3390/nu14071479.
21 Zhang X, Ai F, Li X, et al. Inflammation-induced S100A8 activates Id3 and promotes colorectal tumorigenesis. *Int J Cancer*. 2015;137(12):2803-2814. https://doi.org/10.1002/ijc.29671.
22 Erben U, Loddenkemper C, Doerfel K, et al. A guide to histomorphological evaluation of intestinal inflammation in mouse models. *Int J Clin Exp Pathol*. 2014;7(8):4557-4576.
23 Ruiz PA, Moron B, Becker HM, et al. Titanium dioxide nanoparticles exacerbate DSS-induced colitis: role of the NLRP3 inflammasome. *Gut*. 2017;66(7):1216-1224. https://doi.org/10.1136/gutjnl-2015-310297.
24 Barreau F, Tisseyre C, Menard S, et al. Titanium dioxide particles from the diet: involvement in the genesis of inflammatory bowel diseases and colorectal cancer. *Part Fibre Toxicol*. 2021;18(1):26. https://doi.org/10.1186/s12989-021-00421-2.
25 Wang P, Hu G, Zhao W, et al. Continuous ZnO nanoparticle exposure induces melanoma-like skin lesions in epidermal barrier dysfunction model mice through anti-apoptotic effects mediated by the oxidative stress-activated NF-κB pathway. *J Nanobiotechnol*. 2022;20(1):111. https://doi.org/10.1186/s12951-022-01308-w.
26 Wang P, Zhang L, Liao Y, et al. Effect of intratracheal instillation of ZnO nanoparticles on acute lung inflammation induced by lipopolysaccharides in mice. *Toxicol Sci*. 2020;173(2):373-386. https://doi.org/10.1093/toxsci/kfz234.
27 Chen Y, Ouyang Y, Li Z, et al. S100A8 and S100A9 in cancer. *Biochim Biophys Acta Rev Cancer*. 2023;1878(3):188891. https://doi.org/10.1016/j.bbcan.2023.188891.
28 Pinto ML, Rios E, Duraes C, et al. The two faces of tumor-associated macrophages and their clinical significance in colorectal cancer. *Front Immunol*. 2019;10:1875. https://doi.org/10.3389/fimmu.2019.01875.
29 Dos Anjos CA. F4/80 as a major macrophage marker: the case of the peritoneum and spleen. *Results Probl Cell Differ*. 2017;62:161-179. https://doi.org/10.1007/978-3-319-54090-0_7.
30 Jorch SK, McNally A, Berger P, et al. Complex regulation of alarmins S100A8/A9 and secretion *via* gasdermin D pores exacerbates autoinflammation in familial Mediterranean fever. *J Allergy Clin Immunol*. 2023;152(1):230-243. https://doi.org/10.1016/j.jaci.2023.01.037.
31 Fang X, Lian H, Liu S, et al. A positive feedback cycle between the alarmin S100A8/A9 and NLRP3 inflammasome-GSDMD signalling reinforces the innate immune response in Candida albicans keratitis. *Inflamm Res*. 2023;72(7):1485-1500. https://doi.org/10.1007/s00011-023-01757-5.
32 Bassorgun CI, Unal B, Erin N, et al. S100A8 and S100A9 positive cells in colorectal carcinoma: clinicopathological analysis. *Gastroenterol Res Pract*. 2014;2014:943175. https://doi.org/10.1155/2014/943175.
33 Zeng ML, Zhu XJ, Liu J, et al. An integrated bioinformatic analysis of the S100 gene family for the prognosis of colorectal cancer. *Biomed Res Int*. 2020;2020:4746929. https://doi.org/10.1155/2020/4746929.
34 Chaudhary N, Choudhary BS, Shah SG, et al. Lipocalin 2 expression promotes tumor progression and therapy resistance by inhibiting ferroptosis in colorectal cancer. *Int J Cancer*. 2021;149(7):1495-1511. https://doi.org/10.1002/ijc.33711.
35 Jia SN, Han YB, Yang R, et al. Chemokines in colon cancer progression. *Semin Cancer Biol*. 2022;86(Pt 3): 400-407. https://doi.org/10.1016/j.semcancer.2022.02.007.
36 Liu L, Zhai Z, Wang D, et al. The association between IL-1 family gene polymorphisms and colorectal cancer: a meta-analysis. *Gene*. 2021;769:145187. https://doi.org/10.1016/j.gene.2020.145187.
37 Yu W, Tu Y, Long Z, et al. Reactive oxygen species bridge the gap between chronic inflammation and tumor development. *Oxid Med Cell Longev*. 2022;2022:2606928. https://doi.org/10.1155/2022/2606928.
38 Sreejit G, Flynn MC, Patil M, et al. S100 family proteins in inflammation and beyond. *Adv Clin Chem*. 2020;98:173-231. https://doi.org/10.1016/bs.acc.2020.02.006.
39 Claudia M, Kristin O, Jennifer O, et al. Comparison of fluorescence-based methods to determine nanoparticle uptake by phagocytes and non-phagocytic cells *in vitro*. *Toxicology*. 2017;378:25-36. https://doi.org/10.1016/j.tox.2017.01.001.
40 Romeo D, Nowack B, Wick P. Combined *in vitro-in vivo* dosimetry enables the extrapolation of *in vitro* doses to human exposure levels: a proof of concept based on a meta-analysis of *in vitro* and *in vivo* titanium dioxide toxicity data. *NanoImpact*. 2022;25:100376. https://doi.org/10.1016/j.impact.2021.100376.
41 Correa SF, Macias MFI, Velazquez DKA, et al. Food-grade titanium dioxide (E171) and zinc oxide nanoparticles induce mitochondrial permeability and cardiac damage after oral exposure in rats. *Nanotoxicology*. 2024;18(2):122-133. https://doi.org/10.1080/17435390.2024.2323069.
42 Colin-Val Z, Vera-Marquez CD, Herrera-Rodriguez MA, et al. Titanium dioxide (E171) induces toxicity in H9c2 rat cardiomyoblasts and *ex vivo* rat hearts. *Cardiovasc Toxicol*. 2022;22(8):713-726. https://doi.org/10.1007/s12012-022-09747-5.
43 Li Q, Lin L, Zhang C, et al. The progression of inorganic nanoparticles and natural products for inflammatory bowel disease. *J Nanobiotechnol*. 2024;22(1):17. https://doi.org/10.1186/s12951-023-02246-x.
44 Xu J, Nunez G. The NLRP3 inflammasome: activation and regulation. *Trends Biochem Sci*. 2023;48(4):331-344. https://doi.org/10.1016/j.tibs.2022.10.002.
45 Li Z, Pan H, Yang J, et al. Xuanfei Baidu Formula alleviates impaired mitochondrial dynamics and activated NLRP3 inflammasome by repressing NF-κB and MAPK pathways in LPS-induced ALI and inflammation models. *Phytomedicine*. 2023;108:154545. https://doi.org/10.1016/j.phymed.2022.154545.
46 Li JM, Deng HS, Yao YD, et al. Sinomenine ameliorates collagen-induced arthritis in mice by targeting GBP5 and regulating the P2X7 receptor to suppress NLRP3-related signaling pathways. *Acta Pharmacol Sin*. 2023;44(12):2504-2524. https://doi.org/10.1038/s41401-023-01124-4.
47 Xu Z, Hu H, Wang K, et al. Sinensetin, a polymethoxyflavone from citrus fruits, ameliorates LPS-induced acute lung injury by suppressing Txnip/NLRP3/Caspase-1/GSDMD signaling-mediated inflammatory responses and pyroptosis. *Food Funct*. 2024;15(14):7592-7604. https://doi.org/10.1039/D4FO01704H.
48 Ball DP, Taabazuing CY, Griswold AR, et al. Caspase-1 interdomain linker cleavage is required for pyroptosis. *Life Sci Alliance*. 2020;3(3):e202000664. https://doi.org/10.26508/lsa.202000664.
49 Fu J, Schroder K, Wu H. Mechanistic insights from inflammasome structures. *Nat Rev Immunol*. 2024;24(7):518-535. https://doi.org/10.1038/s41577-024-00995-w.